

1 **Localising individual atoms of tryptophan side chains in the metallo- β -lactamase IMP-1**
2 **by pseudocontact shifts from paramagnetic lanthanoid tags at multiple sites**

3 Henry W. Orton,^{a,*} Iresha D. Herath,^{b,*} Ansis Maleckis,^c Shereen Jabar,^b Monika Szabo,^d Bim
4 Graham,^d Colum Breen,^e Lydia Topping,^e Stephen J. Butler,^e Gottfried Otting^a

5
6 ^a ARC Centre of Excellence for Innovations in Peptide & Protein Science, Research School of
7 Chemistry, Australian National University, Canberra, ACT 2601, Australia

8 ^b Research School of Chemistry, The Australian National University, Sullivans Creek Road,
9 Canberra ACT 2601, Australia

10 ^c Latvian Institute of Organic Synthesis, Aizkraukles 21, LV-1006 Riga, Latvia

11 ^d Monash Institute of Pharmaceutical Sciences, Monash University, Parkville, VIC 3052,
12 Australia

13 ^e Department of Chemistry, Loughborough University, Epinal Way, Loughborough, LE11
14 3TU, United Kingdom

18
19 Correspondence: Gottfried Otting (gottfried.otting@anu.edu.au)

20 * These authors contributed equally to this work.

21
22 **Abstract**

23 The metallo- β -lactamase IMP-1 features a flexible loop near the active site that assumes
24 different conformations in single crystal structures, which may assist in substrate binding and
25 enzymatic activity. To probe the position of this loop, we labelled the tryptophan residues of
26 IMP-1 with 7-¹³C-indole and the protein with lanthanoid tags at three different sites. The
27 magnetic susceptibility anisotropy ($\Delta\chi$) tensors were determined by measuring pseudocontact
28 shifts (PCS) of backbone amide protons. The $\Delta\chi$ tensors were subsequently used to identify
29 the atomic coordinates of the tryptophan side chains in the protein. The PCSs were sufficient
30 to determine the location of Trp28, which is located in the active site loop targeted by our
31 experiments, with high accuracy. Its average atomic coordinates showed barely significant
32 changes in response to the inhibitor captopril. It was found that localisation spaces could be
33 defined with better accuracy by including only the PCSs of a single paramagnetic lanthanoid
34 ion for each tag and tagging site. The effect was attributed to the shallow angle with which

35 PCS isosurfaces tend to intersect if generated by tags and tagging sites that are identical except
36 for the paramagnetic lanthanoid ion.

37

38 **1 Introduction**

39 The metallo- β -lactamase IMP-1 is an enzyme that hydrolyses β -lactams, thus conferring
40 penicillin resistance to bacteria. First identified 30 years ago in the Gram-negative bacteria in
41 early 1990s from *Pseudomonas aeruginosa* and *Serratia marcescens* (Bush 2013), IMP-1 has
42 become a serious clinical problem due to horizontal gene transfer by a highly mobile gene
43 (bla_{IMP-1}) located on an integron (Arakawa et al., 1995), as the bla_{IMP-1} gene has been detected
44 in isolates of *Klebsiella pneumoniae*, *Pseudomonas putida*, *Alcaligenes xylosoxidans*,
45 *Acinetobacter junii*, *Providencia rettgeri*, *Acinetobacter baumannii* and *Enterobacter*
46 *aerogenes* (Ito et al., 1995; Laraki et al., 1999a; Watanabe et al., 1991). Critically, IMP-1
47 confers resistance also to recent generations of carbapenems and extended-spectrum
48 cephalosporins (Laraki et al., 199b; Bush et al., 2010; van Duin et al., 2013).

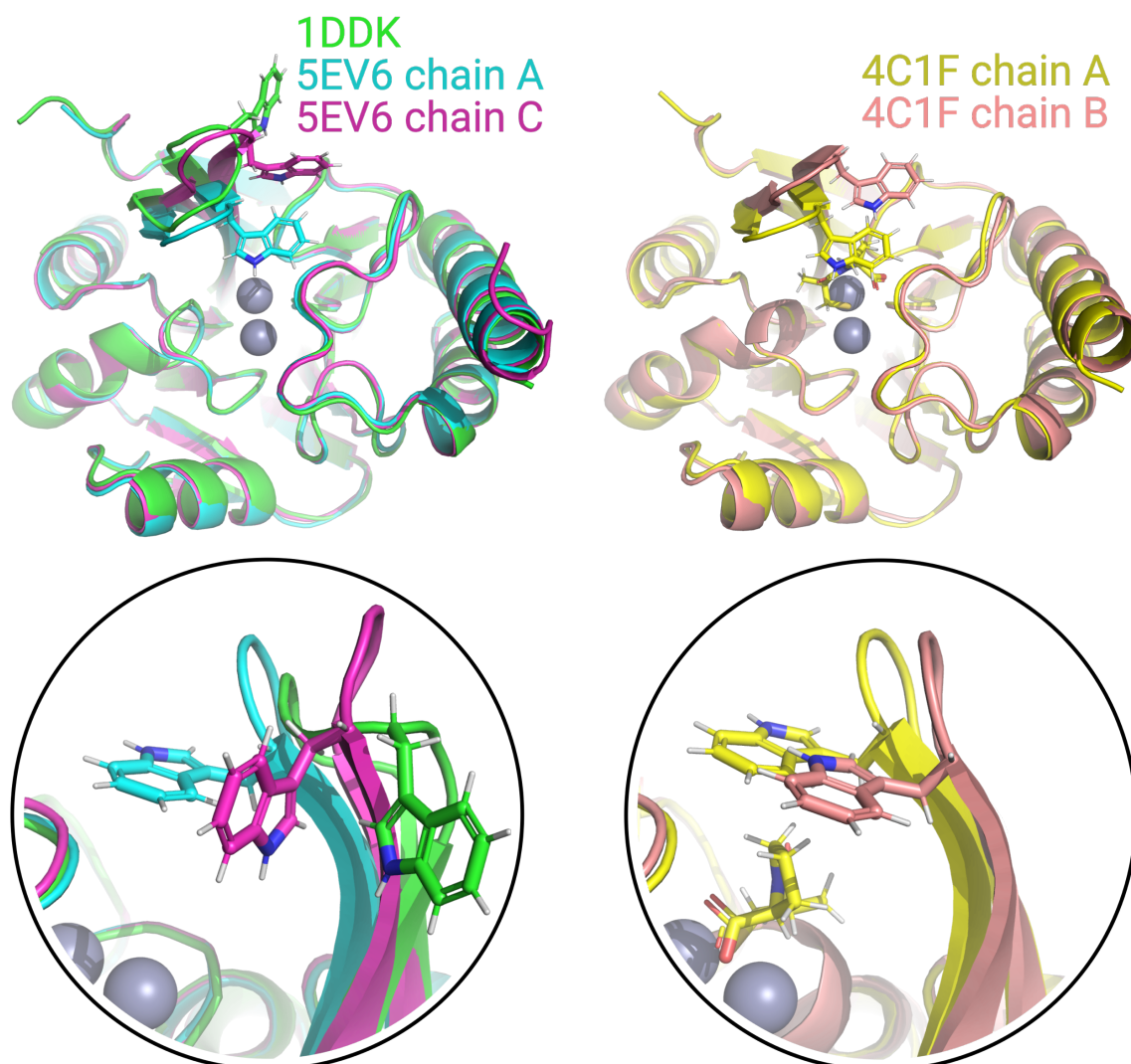
49 Multiple crystal structures have been solved of IMP-1, free and in complex with various
50 inhibitors (Concha et al., 2000; Toney et al., 2001; Moali et al., 2003; Hiraiwa et al., 2014;
51 Brem et al., 2016; Hinchliffe et al., 2016; 2018; Wachino et al., 2019; Rossi et al., 2021). IMP-
52 1 belongs to the subclass B1 of metallo- β -lactamases, which contain two zinc ions bridged by
53 the sulfur atom of a cysteine residue in the active site (Concha, 2000). One of Zn^{2+} ions can
54 readily be replaced by a Fe^{3+} ion (Carruthers et al., 2014). The active site is flanked by a loop
55 (referred to as L3 loop) that contains a highly solvent-exposed tryptophan residue surrounded
56 by glycine residues on either side. Both the loop and the tryptophan residue (Trp28 in the IMP-
57 1-specific numbering used by Concha et al. (2000) and Trp64 in the universal numbering
58 scheme by Galleni et al. (2001)) assume different conformations in different crystal structures,
59 suggesting that the loop acts as a mobile flap to cover bound substrate (Fig. 1). The L3 loop
60 and the functional implication of its flexibility has been studied extensively for different
61 metallo- β -lactamases containing the Gly-Trp-Gly motif in the loop (Huntley et al., 2000; 2003;
62 Moali et al., 2003; Yamaguchi et al., 2015; Palacios et al., 2019; Gianquinto et al., 2020; Softley
63 et al., 2020). Flexibility of the L3 loop is a general feature also of many metallo- β -lactamases
64 without the Gly-Trp-Gly motif and is thought to contribute to the wide range of β -lactam
65 substrates that can be hydrolyzed by the enzymes (González et al., 2016; Linciano et al., 2019;
66 Salimraj et al., 2018). In the case of the metallo- β -lactamase from *B. fragilis*, which is closely
67 related to IMP-1, electron density could be detected for the Gly-Trp-Gly motif in the crystal

68 structure of the protein in the presence (Payne et al., 2003) but not absence of an inhibitor
69 (Concha et al., 1996), and an NMR relaxation study in solution confirmed the increased
70 flexibility of both the L3 loop and, in particular, the sidechain of the tryptophan residue
71 (Huntley et al., 2000). A similar situation prevails in the case of the IMP-1 variant IMP-13,
72 where different crystal structures of the ligand-free protein show the L3 loop in very different
73 conformations, sometimes lacking electron density, while NMR relaxation measurements
74 confirmed the increased flexibility of the loop (Softley et al., 2020).

75 Due to the rigidity of their sidechains, tryptophan residues frequently contribute to the
76 structural stability of three-dimensional protein folds and it is unusual to observe tryptophan
77 sidechains fully solvent-exposed as in the Gly-Trp-Gly motif of substrate-free IMP-1. The
78 functional role of Trp28 in IMP-1 was assessed in an early mutation study by mutating Trp28
79 to alanine and, in a different experiment, eliminating the L3 loop altogether. Enzymatic activity
80 measurements revealed an increase in the Michaelis constant K_m and a decrease in k_{cat}/K_m ratios
81 for all β -lactams tested, illustrating the importance of the Trp28 sidechain for catalytic activity.
82 Complete removal of the L3 loop reduced the k_{cat}/K_m ratios even further, but without
83 completely abolishing the enzymatic activity (Moali et al., 2003).

84

85



86
 87 **Figure 1.** Superimposition of crystal structures of IMP-1 showing structural variation of Trp28
 88 and the associated loop L3. The structures shown are of the Zn^{2+}/Zn^{2+} complex without
 89 inhibitor (green, PDB ID 1DDK, Concha et al., 2000; cyan for chain A and magenta for chain
 90 C, PDB ID 5EV6, Hinchliffe et al., 2016), with bound L-captopril (yellow for chain A and
 91 salmon for chain B, PDB ID 4CIF, Brem et al., 2016). Zn^{2+} ions are represented by grey spheres
 92 and bound captopril is shown in the structure 4CIF chain A.

93
 94 In the crystalline state, the conformation of a solvent-exposed loop is easily impacted
 95 by crystal packing forces. Therefore, it is unclear what the actual conformation of the L3 loop
 96 is in solution. To address this question, we used solution NMR spectroscopy to assess the
 97 location of Trp28 in IMP-1 both in the absence and presence of the inhibitor L-captopril, which
 98 inhibits metallo- β -lactamases by binding to the active-site zinc ions (Brem et al., 2016). The
 99 analysis was hindered by incomplete backbone resonance assignments of IMP-1 attributed to

100 conformational exchange processes in parts of the protein (Carruthers et al., 2014). As it is
101 difficult to accurately position the atoms of a solvent-exposed polypeptide loop in solution by
102 nuclear Overhauser effects (NOE), we used pseudocontact shifts (PCS) generated by
103 lanthanoid ions attached at different sites of IMP-1 to determine the location of Trp28 relative
104 to the core of the protein. PCSs generated by multiple different paramagnetic metal ions or the
105 same metal ion attached at different sites of a protein have previously been shown to allow
106 localizing atoms at remote sites of interest, such as in specific amino acid side chains (Pearce
107 et al., 2017; Lescanne et al., 2018), bound ligand molecules (Guan et al., 2013; Chen et al.,
108 2016) or proteins (Pintacuda et al., 2006; Keizers et al., 2010; de la Cruz et al., 2011;
109 Kobashigawa et al., 2012; Brewer et al., 2015) or for 3D structure determinations of proteins
110 (Yagi et al., 2013; Crick et al., 2015; Pilla et al., 2017).

111 IMP-1 contains six tryptophan residues, each containing several aromatic hydrogens
112 with similar chemical shifts. To increase the spectral resolution in the 2D NMR spectra
113 recorded for PCS measurements, we labelled each tryptophan sidechain with a single ^{13}C atom
114 by expressing the protein in the presence of 7- ^{13}C -indole (Maleckis et al., 2021). The results
115 show that the localization spaces defined by the tryptophan PCSs fully agree with previously
116 determined crystal structures of IMP-1 for all tryptophan residues. They suggest little change
117 in the average conformation of the L3 loop upon binding of captopril. The results illustrate the
118 accuracy with which the positions of individual atoms can be determined by PCSs from
119 lanthanoid tags even in proteins of limited stability.

120

121 **2 Experimental procedures**

122 **2.1 Production, purification and tagging of proteins**

123 **2.1.1 Plasmid constructs and ^{13}C -labelled indole**

124 Three different cysteine mutations (A53C, N172C and S204C) were introduced into the *bla*_{IMP1}
125 gene in the pET-47b(+) plasmid using a modified QuikChange protocol (Qi and Otting, 2019).
126 Deuterated 7- ^{13}C -indole was synthesized as described with deuteration in all positions other
127 than position 7 (Maleckis et al., 2021). The amino acid sequence of the protein was that
128 reported in the crystal structure 4UAM (Carruthers et al., 2014), except that the N-terminal
129 alanine residue was substituted by a methionine to avoid heterogeneity by incomplete
130 processing by amino peptidase.

131

132 **2.1.2 Protein production**

133 Uniformly ^{15}N -labelled samples of the cysteine mutants of IMP-1 were expressed in *E. coli*
134 BL21(DE3) cells. The cells were grown at 37 °C in Luria–Bertani (LB) medium containing 50
135 mgL^{-1} kanamycin until the OD_{600} reached 0.6–0.8 and were then transferred to 300 mL of M9
136 medium ($6 \text{ gL}^{-1} \text{ Na}_2\text{HPO}_4$, $3 \text{ gL}^{-1} \text{ KH}_2\text{PO}_4$, $0.5 \text{ gL}^{-1} \text{ NaCl}$, pH 7.2) supplemented with 1 gL^{-1}
137 of $^{15}\text{NH}_4\text{Cl}$. After induction with isopropyl- β -D-thiogalactopyranoside (IPTG, final
138 concentration 1 mM), the cells were incubated at room temperature for 16 hours. Following
139 centrifugation, the cells were resuspended in buffer A (50 mM HEPES, pH 7.5, 100 μM ZnSO_4)
140 for lysis by a homogeniser (Avestin Emulsiflex C5). The supernatant of the centrifuged cell
141 lysate was loaded onto a 5 mL SP column, the column was washed with 20 column volumes
142 buffer B (same as buffer A but with 50 mM NaCl) and the protein was eluted with a gradient
143 of buffer C (same as buffer A but with 1 M NaCl).

144 IMP-1 samples containing $7\text{-}^{13}\text{C}$ -tryptophan were produced by continuous exchange
145 cell-free protein synthesis (CFPS) from PCR-amplified DNA with eight-nucleotide single-
146 stranded overhangs as described (Wu et al., 2007), using $7\text{-}^{13}\text{C}$ -indole as a precursor for the *in*
147 *vitro* production of tryptophan (Maleckis2021). The CFPS reactions were conducted at 30 °C
148 for 16 h using 1 mL inner reaction mixture and 10 mL outer buffer. Tryptophan was omitted
149 from the mixture of amino acids provided and deuterated $7\text{-}^{13}\text{C}$ -indole was added from a stock
150 solution in 50 % DMSO/50 % H_2O to the inner and outer buffers at a final concentration of
151 0.75 mM. The protein samples were purified as described above. ~5 mg of the indole was
152 required for preparing each NMR sample.

153

154 **2.1.3 Ligation with C2-Ln³⁺ tag**

155 To ensure the reduced state of cysteine thiol groups, the protein samples were treated with 2
156 mM dithiothreitol (DTT) for 1 hour. Subsequently, the DTT was removed using an Amicon
157 ultrafiltration centrifugal tube with a molecular weight cut-off of 10 kDa, concentrating the
158 protein samples to 50 μM in buffer A. The samples were incubated overnight at room
159 temperature with shaking in the presence of five-fold molar excess of C2 tag (Graham et al.,
160 2011; de la Cruz et al., 2011) loaded with either Y^{3+} , Tb^{3+} or Tm^{3+} . Following the tagging
161 reaction, the samples were washed using an Amicon centrifugal filter unit to remove unbound
162 tag and the buffer was exchanged to NMR buffer (20 mM MES, pH 6.5, 100 mM NaCl).

163

164 **2.1.4 Ligation with C12-Ln³⁺ tag**

165 The ligation reaction of IMP-1 N172C with the C12-Ln³⁺ tag loaded with either Y³⁺, Tb³⁺ or
166 Tm³⁺ (Herath et al., 2021) was conducted in the same way as with the C2-Ln³⁺ tags, except that
167 the reactions were carried out in buffer A with the pH adjusted to 7.0.

168

169 2.2 NMR spectroscopy

170 All NMR data were acquired at 37 °C on Bruker 600 and 800 MHz NMR spectrometers
171 equipped with TCI cryoprobes designed for 5 mm NMR tubes, but only 3 mm NMR tubes were
172 used in this project. Protein concentrations were 0.6 mM and 0.2 mM for ¹⁵N-HSQC spectra
173 of samples labelled with the C2 and C12 tag, respectively. The protein concentrations were 0.4
174 mM for ¹³C-HSQC and NOE-relayed ¹³C-HSQC spectra. ¹⁵N-HSQC spectra were recorded at
175 a ¹H-NMR frequency of 800 MHz with $t_{1\max} = 40$ ms, $t_{2\max} = 170$ ms, using a total recording
176 time of 3 h per spectrum. ¹³C-HSQC spectra were recorded with a S³E filter to select the low-
177 field doublet component due to the ¹J_{HC} coupling of the ¹³C-labelled tryptophan side chains.
178 The pulse sequence is shown in Fig. S8 and the spectra were recorded at a ¹H-NMR frequency
179 of 600 MHz using $t_{1\max} = 20$ – 50 ms, $t_{2\max} = 106$ ms and total recording times of 2 h per
180 spectrum. ¹³C-HSQC spectra with NOE relay were recorded without decoupling in the ¹³C-
181 dimension, relying on relaxation and ¹³C equilibrium magnetisation to emphasize the narrow
182 doublet component. The NOE mixing time was 150 ms and the total recording time 3 h per
183 spectrum. The pulse sequence is shown in Fig. S9.

184 To account for uncertainties in concentration measurements, samples with L-captopril
185 were prepared with a nominal ratio of captopril to protein of 1.5:1. In the case of samples
186 tagged with the C2 tag, however, this lead to gradual release of some of the tag, as captopril
187 contains a free thiol group and the disulfide linkage of the C2 tag is sensitive to chemical
188 reduction. To limit this mode of sample degradation, the NOE-relayed [¹³C,¹H]-HSQC spectra
189 were recorded with a smaller excess of captopril.

190

191 2.3 $\Delta\chi$ -tensor fits

192 The experimental PCSs ($\Delta\delta^{\text{PCS}}$) were measured in ppm as the amide proton chemical shift
193 observed in NMR spectra recorded for the IMP-1 mutants A53C, N172C and S204C tagged
194 with Tm³⁺ or Tb³⁺ tags minus the corresponding chemical shift measured of samples made with
195 Y³⁺ tags. The resonance assignments of the wild-type Zn₂ enzyme (BMRB entry 25063) were
196 used to assign the ¹⁵N-HSQC cross-peaks in the diamagnetic state. The program Paramagpy
197 (Orton et al., 2020) was used to fit magnetic susceptibility anisotropy ($\Delta\chi$) tensors to crystal
198 structures of IMP-1 solved in the absence and presence of the inhibitor captopril.

199

200 **3 Results**

201 **3.1 Protein production**

202 Three cysteine mutants of uniformly ^{15}N -labelled IMP-1 were produced *in vivo*, where cysteine
203 residues replaced Ala53, Asn172 and Ser204, respectively. The purified proteins were tagged
204 with C2 tags containing Tb^{3+} or Tm^{3+} as the paramagnetic ions and Y^{3+} as the diamagnetic
205 reference. Samples of the uniformly ^{15}N -labelled mutant N172C were also ligated with C12
206 tags containing the same set of metal ions. The chemical structures of the tags are depicted in
207 Fig. S1. To record ^{13}C - ^1H correlation spectra of the tryptophan side chains with minimal
208 spectral overlap, additional samples of the cysteine mutants were produced with selectively
209 ^{13}C -labelled tryptophan residues. These samples were produced by cell-free protein synthesis
210 in the presence of 7- ^{13}C indole, deuterated except at the 7 position, with the omission of
211 tryptophan, using a recently established protocol (Maleckis et al., 2021). The residual activity
212 of tryptophan synthase in the cell-free extract was sufficient to produce tryptophan from the
213 added ^{13}C -labelled indole. The resulting tryptophan residues contained a ^{13}C - ^1H group in
214 position 7 ($^{13}\text{C}^{\zeta 2}$ and $^1\text{H}^{\zeta 2}$ in IUPAC nomenclature; Markley et al., 1998) and deuterons at all
215 other hydrogen positions of the indole ring except for the H^{N} atom ($\text{H}^{\varepsilon 1}$ in IUPAC
216 nomenclature). The cell-free expression yielded about 2 mg of purified protein per millilitre of
217 inner cell-free reaction mixture. Mass spectrometry indicated that the tryptophan residues of
218 IMP-1 were $^{13}\text{C}/^2\text{H}$ -labelled with about 80 % labelling efficiency at each of the six tryptophan
219 positions (Fig. S2). The purified proteins were ligated with C2- Ln^{3+} tags containing either Tb^{3+} ,
220 Tm^{3+} or Y^{3+} as in the case of the ^{15}N -labelled samples. Ligation yields with the C2 tags were
221 practically complete as indicated by mass spectrometry (Fig. S2). The ligation yield of the
222 N172C mutant with C12 tags was about 90 % (Herath et al., 2021).

223

224 **3.2 NMR experiments and resonance assignments**

225 [^{15}N , ^1H]-HSQC spectra were measured of the tagged proteins in the free state and in the
226 presence of L-captopril (Fig. S3–S7). ^1H PCSs of backbone amide protons measured in these
227 spectra were used to establish the $\Delta\chi$ tensors relative to the protein. The resonance assignment
228 of the [^{15}N , ^1H]-HSQC spectra in the presence of inhibitor was transferred from the
229 corresponding spectra recorded in the absence of inhibitor. As no resonance assignments could
230 reliably be made in this way in areas of spectral overlap, fewer resonance assignments were
231 available in the presence than absence of inhibitor. Furthermore, due to captopril releasing

232 some of the C2 tags from the protein by breaking the disulfide bridge of the tag attachment,
233 spectra recorded in the presence of captopril contained additional cross-peaks from
234 diamagnetic protein.

235 To obtain tagged protein that is inert against chemical reduction, we also attached the
236 C12 tag to the mutant N172C. This tag, however, caused the appearance of additional peaks in
237 the [¹⁵N,¹H]-HSQC spectra (Fig. S6). The additional peaks appeared in different sample
238 preparations, indicating sample degradation or perturbation of the local protein structure by the
239 tag. We therefore based the rest of the work mainly on the PCSs obtained with the C2 tags.
240 Tables S1 and S2 list the PCSs of the backbone amides measured in the absence and presence
241 of captopril.

242 ¹H PCSs of the tryptophan H^{ε2} protons were measured in [¹³C,¹H]-HSQC spectra
243 recorded with S³E spin-state selection element (Meissner et al., 1997) in the ¹³C dimension to
244 select the slowly relaxing components of the doublets split by ¹J_{HC} couplings. Cross-peaks were
245 observed for all six tryptophan residues except for the mutant N172C, which displayed cross-
246 peaks of only five tryptophan indoles (Fig. 2). The missing signal was attributed to Trp176
247 because of its close proximity to the tagging site. The indole H^{ε1} proton is located within 2.9 Å
248 of the H^{ε2} proton and the NOE between both protons was readily observed in a [¹³C,¹H]-HSQC
249 experiment with NOE relay (Fig. 2). The H^{ε1} chemical shifts afforded better spectral resolution
250 than the H^{ε2} resonances. Comparison of the predicted and observed PCSs yielded resonance
251 assignments of all tryptophan H^{ε1} cross-peaks with particular clarity in the NOE-relayed
252 [¹³C,¹H]-HSQC spectrum (Fig. 2). In addition, the assignment was supported by paramagnetic
253 relaxation enhancements (for example, Trp88 is near residue 53 and therefore its cross-peaks
254 were strongly attenuated in the paramagnetic samples of the A53C mutant). Different PCSs
255 were observed for all six tryptophan sidechains and different PCSs were observed for the H^{ε2}
256 and H^{ε1} protons within the same indole sidechain. Each of the tryptophan sidechains showed
257 PCSs in most, if not all, of the mutants. As the L3 loop is near residue 172, the mutant N172C
258 endowed Trp28 with particularly large PCSs. Tables S3 and S4 report the PCSs measured in
259 this way for the samples labelled with C2 tags.

260 In contrast, assigning the indole N-H groups in the [¹⁵N,¹H]-HSQC spectra was much
261 more difficult because IMP-1 is a protein prone to showing more than a single peak per proton
262 (Fig. S5). In particular, the [¹⁵N,¹H]-HSQC spectrum of wild-type IMP-1 selectively labelled
263 with ¹⁵N-tryptophan displayed five intense and at least three weak N^{ε1}-H^{ε1} cross-peaks
264 (Carruthers 2014) and the [¹⁵N,¹H]-HSQC spectra of the tagged cysteine mutants showed

265 evidence of heterogeneity too (Fig. S5). Nonetheless, the five most intense $N^{\epsilon 1}-H^{\epsilon 1}$ cross-peaks
266 could be assigned by comparison to the PCSs observed in the NOE-relayed [$^{13}C, ^1H$]-HSQC
267 spectrum and this assignment was used to measure the PCSs of the tryptophan $H^{\epsilon 1}$ resonances
268 in the mutant N172C tagged with C12 tag (Fig. S7; Table S4).

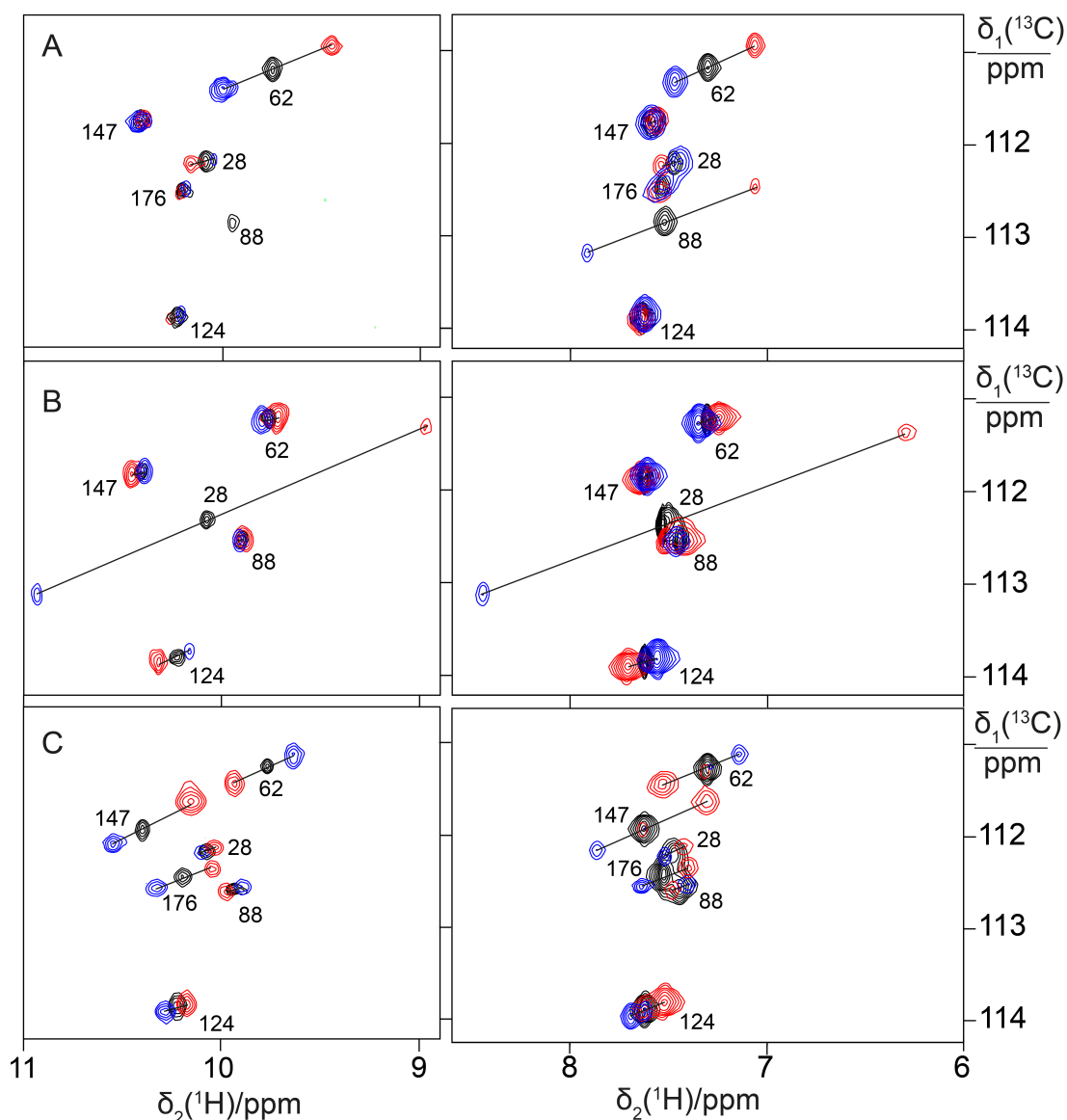
269 Spectra recorded in the presence of L-captopril were very similar to those recorded
270 without the inhibitor, except that some new, narrow C-H cross-peaks appeared in the [$^{13}C, ^1H$]-
271 HSQC spectra of the mutants A53C and S204C, which were suggestive of protein degradation
272 (Fig. 3). We consequently used the better-resolved indole H^N cross-peaks to identify the correct
273 parent C-H cross-peaks. The chemical shifts of the tryptophan sidechains changed very little
274 in response to the presence of L-captopril, except for the ^{13}C -chemical shift of Trp28, which is
275 nearest to the ligand binding site. The PCSs of the indole protons measured in the presence of
276 the inhibitor are listed in Tables S5 and S6.

277

278 **3.2 $\Delta\chi$ -tensor fits**

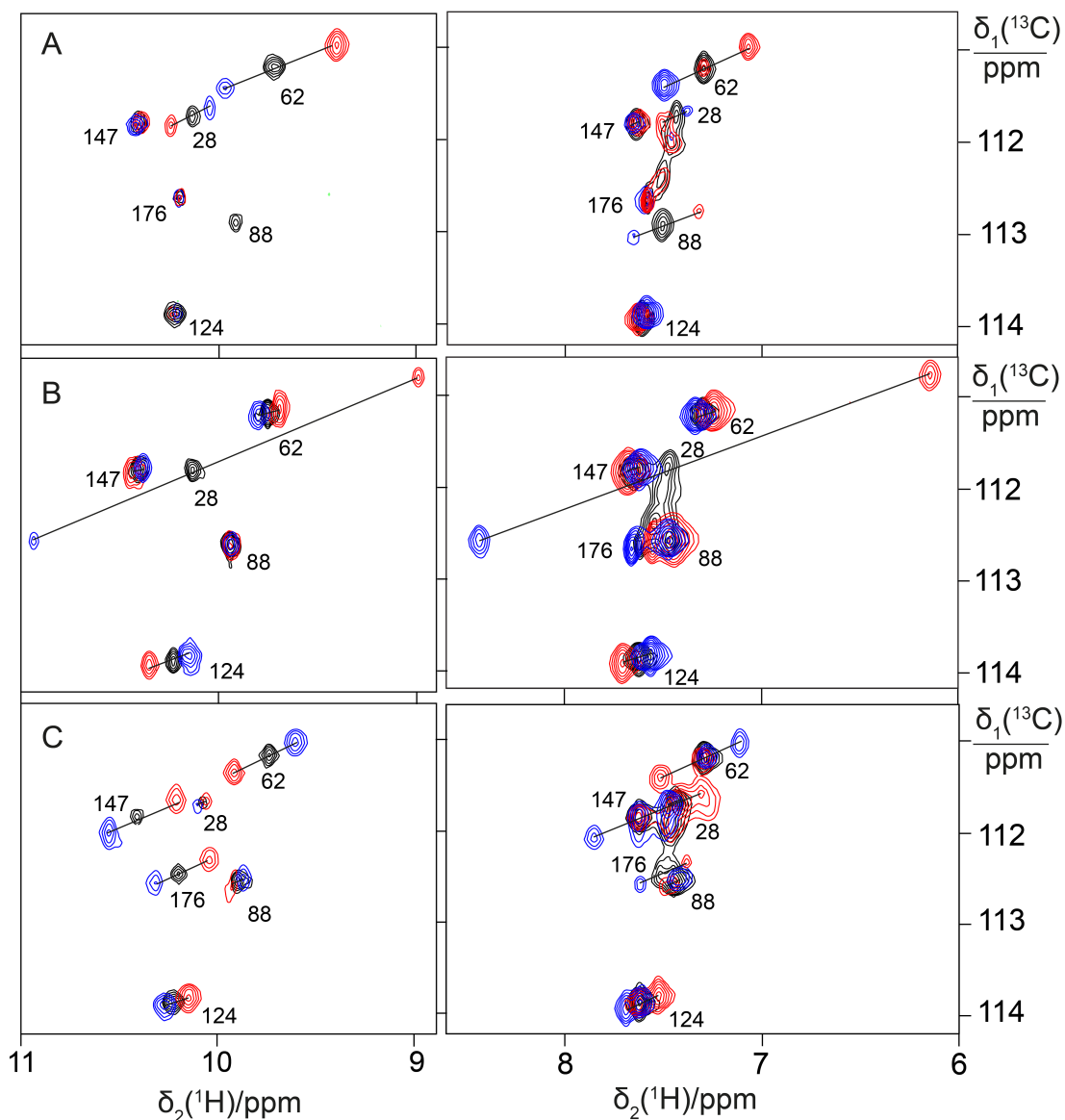
279 The $\Delta\chi$ -tensor parameters were determined using the program Paramagpy (Orton et al., 2020),
280 using all available 1H PCSs measured of backbone amides. Comparing the $\Delta\chi$ tensor fits to the
281 crystal structures 5EV6 chains A and C (Hinchliffe et al., 2016) and 1DDK (Concha et al.,
282 2000) of the free protein, the chain A of the structure 5EV6 proved to produce the smallest Q
283 factor by a small margin (Fig. S10) and was used as the reference structure of the free protein
284 for the subsequent evaluation. Similarly, chain A of the co-crystal structure published with the
285 inhibitor L-captopril (PDB ID: 4C1F; Brem et al., 2016) on average delivered better fits than
286 chain B and was used as the reference structure for the NMR data recorded in the presence of
287 L-captopril. The $\Delta\chi$ -tensor fits of each mutant and tag used a common metal position for the
288 data obtained with the Tb^{3+} and Tm^{3+} tags. The fits positioned the paramagnetic centres at
289 distances between 8.9 and 10.2 Å from the C^α atom of the tagged cysteine residues, which is
290 compatible with the chemical structure of the C2-tag. Figure 4 shows the correlations between
291 back-calculated and experimental PCSs and Table S7 reports the fitted $\Delta\chi$ tensor parameters.
292 Very similar Q factors were obtained when using the PCSs measured in the absence of inhibitor
293 to fit the $\Delta\chi$ tensor to the co-crystal structure 4C1F or the PCSs measured in the presence of
294 inhibitor to fit the $\Delta\chi$ tensor to the crystal structure of the free protein. This indicates that the
295 protein structure did not change very much in response to inhibitor binding. This conclusion
296 was also indicated by the similarity between the backbone PCSs observed with and without
297 inhibitor (Fig. S11).

298 The $\Delta\chi$ tensors obtained with the Tb^{3+} tags were larger than those obtained with the
 299 Tm^{3+} tags, which is also reflected by the consistently larger PCSs observed in the ^{13}C - ^1H
 300 correlation spectra of Fig. 2 and 3. The fits of $\Delta\chi$ tensors to the protein backbone also yielded
 301 better Q factors for PCSs generated by Tb^{3+} than Tm^{3+} ions. Therefore, we determined the
 302 localization spaces of the tryptophan sidechains in the first instance by using their ^1H PCSs
 303 measured with Tb^{3+} tags only.
 304

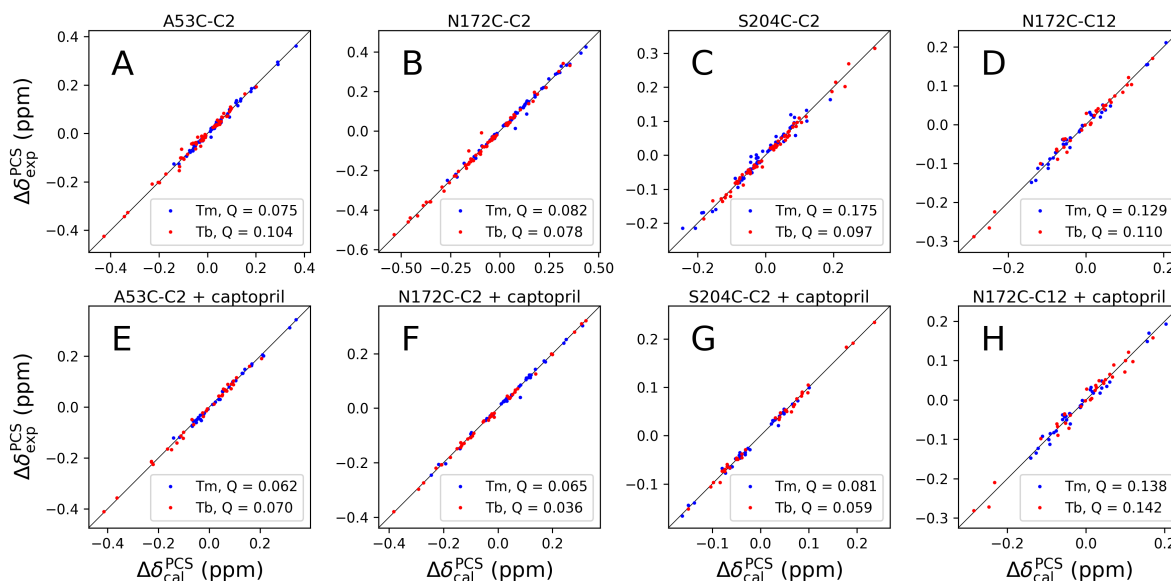


305
 306 **Figure 2.** PCSs observed in ^{13}C - ^1H correlation spectra of 0.4 mM solutions of IMP-1 mutants
 307 labelled with 7- ^{13}C -tryptophan (deuterated in the indole positions 2, 4, 5 and 6) and tagged with
 308 C2-Ln^{3+} tags. The plots show superimpositions of spectra recorded with diamagnetic (C2-Y^{3+} ,
 309 black) or paramagnetic (C2-Tb^{3+} , red; C2-Tm^{3+} , blue) tags. All spectra were recorded with
 310 spin-state selection in the ^{13}C -dimension to record the narrow low-field component of each

311 ^{13}C -doublet. Right panels: $^{13}\text{C}, ^1\text{H}$ -HSQC spectra. Left panels: $^{13}\text{C}, ^1\text{H}$ -HSQC spectra with
 312 150 ms NOE relay to record the $\text{H}^{\epsilon 1}$ resonances of the tryptophan side chains. PCSs are
 313 indicated by lines connecting the peaks of paramagnetic and diamagnetic samples. The cross-
 314 peaks are assigned with the residue number of the individual tryptophan residues. (A) Mutant
 315 A53C. (B) Mutant N172C. (C) Mutant S204C.



316
 317 **Figure 3.** PCSs observed in ^{13}C - ^1H correlation spectra of 0.4 mM solutions of IMP-1 mutants
 318 recorded in the presence of L-captopril. Protein preparations and experimental parameters were
 319 the same as in Fig. 2. Spectra recorded with diamagnetic ($\text{C}2\text{-Y}^{3+}$, black) or paramagnetic ($\text{C}2\text{-Tb}^{3+}$, red;
 320 $\text{C}2\text{-Tm}^{3+}$, blue) tags are superimposed. Right column: $^{13}\text{C}, ^1\text{H}$ -HSQC spectra. Left
 321 column: $^{13}\text{C}, ^1\text{H}$ -HSQC spectra with 150 ms NOE. (A) Mutant A53C. (B) Mutant N172C. (C)
 322 Mutant S204C.



323

324 **Figure 4.** Correlations between back-calculated and experimental ^1H PCSs measured of
 325 backbone amides of IMP-1 with C2 tags at three different sites (positions 53, 172 and 204) and
 326 the C12 tag in position 172. Red and blue data points correspond to the PCS data obtained with
 327 Tb^{3+} and Tm^{3+} tags, respectively. (A) Mutant A53C with C2 tag. (B) Mutant N172C with C2
 328 tag. (C) Mutant S204C with C2 tag. (D) Mutant N172C with C12 tag. (E) Same as (A) but in
 329 the presence of captopril. (F) Same as (B) but in the presence of captopril. (G) Same as (C) but
 330 in the presence of captopril. (H) Same as (D) but in the presence of captopril. PCS data in (A)–
 331 (D) were used to fit $\Delta\chi$ tensors to the structure 5EV6. PCS data in (E)–(F) were used to fit $\Delta\chi$
 332 tensors to the structure 4C1F.

333

334 3.3 Determining the localisation spaces of tryptophan sidechains

335 The $\Delta\chi$ tensors determined of backbone amides not only enabled the resonance assignment of
 336 the tryptophan sidechains by comparing back-calculated with experimental PCSs, but also
 337 allowed translation of the indole PCSs into restraints that define the locations of the tryptophan
 338 $\text{H}^{\epsilon 2}$ and $\text{H}^{\epsilon 1}$ atoms with respect to the rest of the protein. The concept of localising nuclear spins
 339 by PCSs that are generated by lanthanoid tags at different sites is well-established (see, e.g.,
 340 Yagi et al., 2013; Lescanne et al., 2018; Zimmermann et al., 2019). It can be visualised by
 341 representing each PCS restraint by the corresponding PCS isosurface, which comprises all
 342 points in space where this PCS value is generated by the $\Delta\chi$ tensor (Fig. 5). With PCS restraints
 343 from two different metal sites, the intersection between the respective isosurfaces defines a
 344 line. The intersection of this line with the PCS isosurface from a third $\Delta\chi$ tensor defines two
 345 points. While a fourth $\Delta\chi$ tensor could unambiguously produce a single solution, a fourth tensor

346 may not be required if one of these two points is incompatible with the covalent structure of
347 the protein. In favourable circumstances, the constraints imposed by the covalent structure may
348 even allow the accurate positioning of nuclear spins by PCSs generated from only two different
349 $\Delta\chi$ tensors (Pearce et al., 2017). Therefore, the present study was successful with only three
350 different tagging sites. Figure S12 illustrates the concept for the Trp28 $H^{\epsilon 1}$ atom.

351 The spatial definition of the intersection point defined by the PCS isosurfaces depends
352 on the experimental uncertainties in a non-isotropic way, as the PCS isosurfaces rarely intersect
353 in an orthogonal manner and the PCS gradients differ for each $\Delta\chi$ tensor. To capture a
354 localisation space, which allows for the experimental uncertainty in the measured PCS data,
355 we mapped the spatial field of root-mean-squared deviations (RMSD) between experimental
356 and calculated PCS values and defined the boundary of the localisation space by a maximal
357 RMSD value. In addition, uncertainties in the $\Delta\chi$ tensors were propagated by averaging over
358 the results from 20 $\Delta\chi$ -tensor fits performed with random omission of 20 % of the backbone
359 PCS data. In the present work, the routine for defining the localisation space was implemented
360 as a script in the software Paramagpy (Orton et al., 2020). Figure 6 shows the resulting
361 localisation spaces for the $H^{\epsilon 1}$ and $H^{\zeta 2}$ atoms of Trp28, using the PCS data obtained for the
362 three cysteine mutants A53C, N172C and S204C with the C2-Tb³⁺ tag as well as the N172C
363 mutant with the C12-Tb³⁺ tag.

364 The localisation spaces found for the $H^{\epsilon 1}$ and $H^{\zeta 2}$ atoms of Trp28 were clearly different.
365 Furthermore, the distance between them corresponded closely to the distance expected from
366 the chemical structure of the indole ring (2.9 Å). The irregular shapes of the localisation spaces
367 displayed in Fig. 5 purely reflect the relative geometry of the intersecting PCS isosurfaces and
368 do not take into account any dynamic flexibility of the L3 loop or protein structure. In
369 particular, the relevant PCS isosurfaces associated with the C2 tag at sites N172C and S204C
370 intersect at a shallow angle, which leads to the elongated shape of the localisation space for the
371 Trp28 $H^{\zeta 2}$ atom (Fig. S12). For the nitrogen-bound $H^{\epsilon 1}$ atom, the localisation space was
372 restricted further by the additional data obtained with the C12 tag at site N172C (Fig. 6).
373 Calculating the localisation spaces from the Tm³⁺ data yielded very similar results (Fig. S13).
374 The agreement of the localisation spaces of Trp28 with chain A of the previously published
375 crystal structure 5EV6 is excellent and they are clearly incompatible with the conformations
376 observed in chain C of the same structure or in the structure 1DDK (Fig. 1).

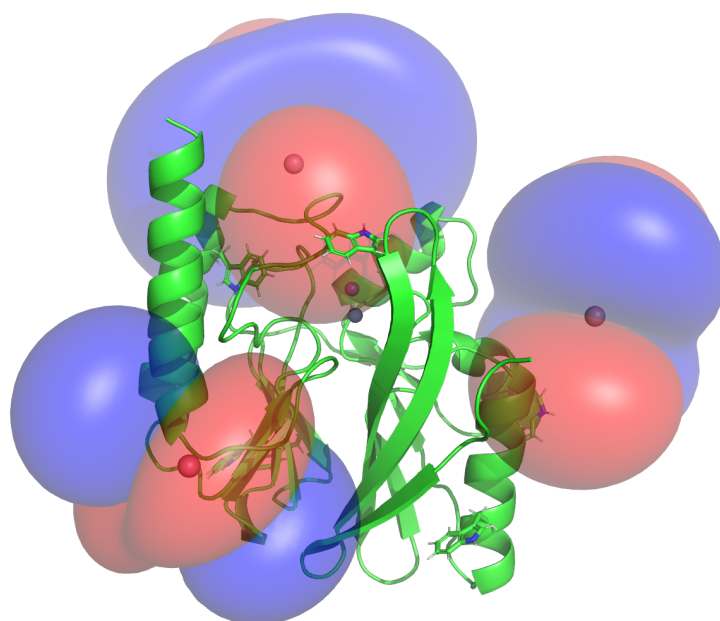
377 Due to close proximity to the C2 tags in the N172C mutant, the largest PCSs were
378 observed for Trp28 $H^{\epsilon 1}$ but, in the absence of captopril, their exact magnitude appeared about

379 0.3 ppm smaller in the [¹⁵N,¹H]-HSQC (Fig. S5b) than the NOE-relayed [¹³C,¹H]-HSQC (Fig.
380 2B) spectrum. The centre of the localisation space of Trp28 H^{ε1} moved to a slightly more open
381 L3 loop conformation when using the smaller PCS detected in the [¹⁵N,¹H]-HSQC spectrum
382 of the N172C mutant labelled with the C2-Tb³⁺ tag. The space still encompassed the
383 coordinates observed in the structure 5EV6, limiting the significance of this difference in PCS.
384

385 **3.4 Defining the localisation space with one versus two lanthanoid ions in the same tag** 386 **and at the same site**

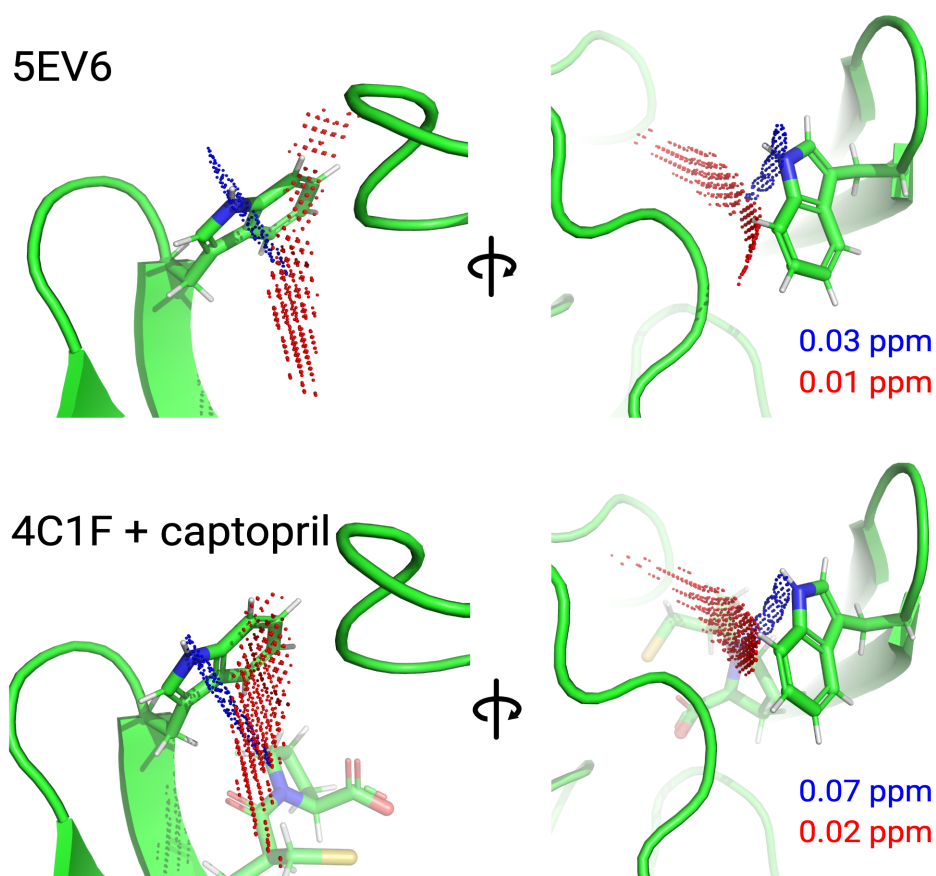
387 Unexpectedly, determining separate localisation spaces from the Tm³⁺ and Tb³⁺ datasets
388 yielded more plausible results than when both datasets were used simultaneously. Careful
389 inspection showed that the close alignment of the $\Delta\chi$ tensors of the Tm³⁺ and Tb³⁺ data resulted
390 in particularly shallow intersection angles of the respective PCS isosurfaces. In calculating the
391 localisation space of Trp28, the PCS isosurfaces arising from the N172C mutant carried by far
392 the greatest weight as this site is closer to residue 28 than the sites 53 and 204. Therefore, the
393 Tm³⁺ and Tb³⁺ data from the N172C mutant dominated the PCS RMSD calculation and the
394 intersection between the associated isosurfaces pulled the final localisation space to a
395 structurally implausible location, which was unstable with respect to small perturbations in $\Delta\chi$ -
396 tensor orientations associated with the tensors at site 172. In contrast, considering the Tm³⁺ and
397 Tb³⁺ datasets separately allowed the localisation spaces to be determined by the intersections
398 with PCS isosurfaces from the other sites. The resulting localisation spaces consistently were
399 compatible with crystal structures.

400



401

402 **Figure 5.** PCS isosurfaces of the IMP-1 mutants A53C, N172C and S204C plotted on the
 403 crystal structure 5EV6. The respective $\Delta\chi$ tensors were determined from the ^1H PCSs measured
 404 of backbone amides. Blue/red isosurfaces correspond to PCSs of ± 1.0 ppm, respectively,
 405 generated with C2-Tb $^{3+}$ tags.
 406
 407



408
 409 **Figure 6.** Localisation space of the sidechain of Trp28 defined by the PCSs from tags in the
 410 IMP-1 mutants A53C, N172C and S204C. Red and blue points outline localisation spaces
 411 determined for the H $^{\zeta 2}$ and H $^{\epsilon 1}$ atoms, respectively. The localisation space of the H $^{\zeta 2}$ atom was
 412 defined by the PCSs and $\Delta\chi$ tensors determined for the Tb $^{3+}$ -loaded C2 tags, while the
 413 localisation space of the H $^{\epsilon 1}$ atom was restricted by additional data obtained with C12-Tb $^{3+}$ tag
 414 at site N172C. The boundaries of the respective localisation spaces displayed are defined by
 415 the PCS RMSD values indicated in ppm. The top panel depicts the localisation spaces
 416 determined for the free protein plotted on chain A of the crystal structure 5EV6 depicted in two
 417 different orientations. The lower panel depicts the localisation spaces determined in the
 418 presence of captopril plotted on chain A of the crystal structure 4C1F.
 419

420 **3.5 L3 loop conformation in the presence of L-captopril**

421 Figure 6 shows that, within the uncertainty of the experiments, the localisation space of the
422 indole sidechain of Trp28 is invariant with respect to the presence or absence of captopril.
423 Conservation of the L3 loop conformation with and without inhibitor is supported by the close
424 similarity in all the PCSs observed for Trp28 in the NOE-relayed [^{13}C , ^1H]-HSQC spectra (Fig.
425 2 and 3). In the [^1H , ^{15}N]-HSQC spectra of the mutant N172C with C2 tag, however, the PCSs
426 observed for Trp28 $\text{H}^{\epsilon 1}$ appeared somewhat smaller without than with captopril (Fig. S5b). As
427 the PCSs of backbone amides were very similar in the absence and presence of the inhibitor
428 (Fig. S11), this difference in PCS suggests a change in L3 loop conformation that did not arise
429 in the selectively ^{13}C -labelled samples. As discussed above, using the smaller PCS of Trp28
430 $\text{H}^{\epsilon 1}$ did not sufficiently change its localisation space in the free protein to render it incompatible
431 with the coordinates of the structure 5EV6. We therefore have little evidence for a significant
432 conformational change of the L3 loop between the free and bound state.

433 The cross-peak intensities of the Trp28 sidechain resonances are relatively weak
434 compared with those of the other tryptophan sidechains, suggesting that Trp28 is subject to
435 dynamics that broaden its resonances. Its cross-peaks appeared slightly weaker in the presence
436 than in the absence of inhibitor (Fig. 2 and 3), suggesting a change in dynamics caused by the
437 inhibitor binding. Previous NMR studies of metallo- β -lactamases reported faster $R_2(^{15}\text{N})$
438 relaxation rates of the L3-loop tryptophan sidechain in the presence than in the absence of
439 inhibitor, which was attributed to dampened dynamics (Huntley et al., 2000; Softley et al.,
440 2020). In the presence of dynamics, the localisation spaces determined in the present work
441 must be considered averages that do not report on the amplitude or direction of motions.

442

443 **3.6 Localisation spaces of tryptophan side chains other than Trp28**

444 As the tagging sites had been designed to analyse the conformation of the L3 loop, they were
445 positioned at similar distances from the L3 loop and therefore not optimal for determining
446 localisation spaces of the other tryptophan residues. Nonetheless, clear differences were
447 observed in the PCSs of the $\text{H}^{\epsilon 2}$ and $\text{H}^{\epsilon 1}$ atoms (Fig. 2), allowing the separation of the respective
448 localisation spaces, which also proved to be in excellent agreement with the conformations of
449 the side-chain indoles of Trp62, Trp124 and Trp147 as found in the crystal structure (Fig. S14),
450 whereas the data were insufficient to determine the sidechain conformation of Trp176.

451

452 **4 Discussion**

453 The L3 loop of metallo- β -lactamases is known to be flexible and, in the specific case of IMP-
454 1, significantly assists in substrate binding and enzymatic activity (Moali et al., 2003). As the
455 substrate is sandwiched between the di-zinc site and the L3 loop, it is tempting to think that the
456 loop opens up for substrate binding and product release while it may be closed during the
457 enzymatic reaction to hold the substrate and reaction intermediate in place. In contrast, some
458 of the conformations observed in crystal structures of IMP-1 obtained in the presence and
459 absence of the inhibitor L-captopril, revealed the loop in almost identical conformations (Brem
460 et al., 2016). This observation is inconclusive, however, as the L3 loop forms more extensive
461 intermolecular contacts with neighbouring protein molecules in the crystal lattice than
462 intramolecular contacts. In addition, other crystal structures observed the loop to move by
463 almost 3 Å in response to a different inhibitor (Concha et al., 2000). This prompted us to probe
464 its actual location in the absence of crystal packing forces in solution, a task which is difficult
465 to tackle by traditional NMR spectroscopic methods that rely on short-range NOEs.

466 Our results show that by furnishing IMP-1 with paramagnetic lanthanoid tags, the
467 coordinates of the indole sidechain of Trp28, which is a key residue near the tip of the loop,
468 can be determined with remarkable accuracy even in the free protein, where the available
469 crystal structures position the L3 loop in a conformation without any direct contacts with the
470 core of the protein. Indeed, the localisation space identified by the NMR data of the free protein
471 proved to be sufficiently well-defined to discriminate between different crystal structures of
472 IMP-1, as well as between different chains in the same asymmetric crystal unit. For example,
473 the sidechain orientation of Trp28 observed in $[\text{Fe}^{3+}, \text{Zn}^{2+}]$ -IMP-1 (4UAM; Carruthers et al.,
474 2014) proved to be in poor agreement with the PCS data, whereas the data were in full
475 agreement with chain A in the structure 5EV6 of $[\text{Zn}^{2+}, \text{Zn}^{2+}]$ -IMP-1 without inhibitor
476 (Hinchliffe et al., 2016) and chain A in the structure 4C1F with bound L-captopril (Brem et al.,
477 2016). This highlights the outstanding capacity of PCSs to assess small conformational
478 differences.

479 The approach of using PCSs for local structure determination is particularly appealing
480 in the case of difficult proteins such as IMP-1, where the sequence-specific NMR resonance
481 assignments are incomplete due to line-broadening attributable to motions in the μs – ms time
482 range and additional signals are observed that either stem from protein degradation, misfolding
483 or alternative conformations in slow exchange with the main structure. Notably, all information
484 required to establish the $\Delta\chi$ tensors could be obtained from resolved cross-peaks observed in
485 sensitive $^{15}\text{N}, ^1\text{H}$ -HSQC spectra. Similarly, the localisation information of the tryptophan

486 sidechains could be obtained from sensitive ^{13}C - ^1H and ^{15}N - ^1H correlation spectra. Positioning
487 the lanthanoid tags relatively far from the substrate binding site avoided direct interference
488 with the binding loop structure.

489 In the face of additional signals from minor species, site-selective ^{13}C -labelling of the
490 tryptophan sidechains was particularly helpful for simplifying the $[^{13}\text{C},^1\text{H}]$ -HSQC spectra.
491 Gratifyingly, this could be achieved by providing suitably labelled indole without having to
492 synthesise the full amino acid (Maleckis et al., 2021).

493 It has been pointed out previously that the accuracy with which localisation spaces can
494 be determined is best when PCS isosurfaces intersect in an orthogonal manner (Pintacuda et
495 al., 2006; Lescanne et al., 2018; Zimmermann et al., 2019). In the present work, we found that,
496 counterintuitively, the provision of additional data can considerably degrade the accuracy of
497 the localisation space. This effect arises when PCS isosurfaces intersect at a shallow angle, as
498 the location of these intersections becomes very sensitive with regard to small errors in the
499 relative orientations of the underpinning $\Delta\chi$ tensors. Shallow intersection angles of PCS
500 isosurfaces are common, when two PCS datasets are from tags and tagging sites that differ only
501 in the identity of the paramagnetic metal ion in the tag. This situation commonly generates $\Delta\chi$
502 tensors of different magnitude and sign, but closely similar orientation (Bertini et al., 2001; Su
503 et al., 2008; Keizers et al., 2008; Man et al., 2010; Graham et al., 2011; Joss et al., 2018;
504 Zimmermann et al., 2021). Therefore, while the use of Tm^{3+} and Tb^{3+} tags is helpful for
505 assigning the cross-peaks in the paramagnetic state, more robust results are obtained by using
506 only one of these data sets for calculating the localisation space. Good localisation spaces were
507 thus obtained by using only PCSs measured for Tb^{3+} tags (Fig. 6) or only PCSs measured for
508 Tm^{3+} tags (Fig. S12). In contrast, however, very different tags attached at the same site, such
509 as the C2 and C12 tags installed in the mutant N172C, produced independent $\Delta\chi$ -tensor
510 orientations and therefore contributed positively to localising the Trp28 $\text{H}^{\text{e}1}$ atom.

511 In principle it is inappropriate to explain a set of PCSs by a single $\Delta\chi$ tensor, if they are
512 generated by a lanthanoid tag attached via a flexible linker, which positions the lanthanide ions
513 at variable coordinates relative to the protein. In this situation, fitting a single $\Delta\chi$ tensor
514 amounts to an approximation. The effective $\Delta\chi$ tensors obtained in this way, however, can
515 fulfill the PCSs remarkably well (Shishmarev and Otting, 2013), as illustrated by the low Q
516 factors obtained in this work (Fig. 4), and the localisation spaces obtained for the tryptophan
517 sidechains are correspondingly well defined.

518 The present work employed ^1H PCSs only, although PCSs were also observed in the

519 indirect dimensions of the [¹³C,¹H]-HSQC and [¹⁵N,¹H]-HSQC spectra. We made this choice
520 because the paramagnetic tags give rise to weak molecular alignments in the magnetic field,
521 which result in residual anisotropic chemical shifts (RACS). The effect is unimportant for ¹H
522 spins but significant for nuclear spins with large chemical shift anisotropy (CSA) tensors such
523 as backbone nitrogens and aromatic carbons. Correcting for the RACS effect is possible with
524 prior knowledge of the CSA tensors and bond orientations (John et al., 2005). We therefore
525 chose not to measure PCSs of the heteronuclear spins in favour of improving sensitivity by
526 accepting a lower spectral resolution in the indirect dimensions.

527 Finally, the C12 tag was designed specifically with the intent to produce a more rigid
528 tether to the protein than the C2 tag, but this did not result in larger $\Delta\chi$ tensors (Table S7) and
529 the NMR spectra of IMP-1 N172C displayed more heterogeneity with the C12 than the C2 tag,
530 suggesting that the shorter and more rigid tether combined with the fairly high molecular
531 weight of the cyclen-lanthanoid complex may have perturbed the protein structure to some
532 degree.

533

534 **5 Conclusion**

535 The current work illustrates how $\Delta\chi$ tensors from paramagnetic lanthanoid ion tags installed at
536 three different sites of the protein can be used to probe the conformation of a selected site in
537 solution in unprecedented detail, provided the structure of most of the protein is known with
538 high accuracy to allow fitting effective $\Delta\chi$ tensors of high predictive value. Importantly,
539 however, the method is easily compromised, if two PCS isosurfaces intersect at a shallow angle
540 as, in this situation, inaccuracies in $\Delta\chi$ tensor determinations have an outsized effect on
541 positioning the localisation spaces defined by the PCSs. Therefore, improved results were
542 obtained by not combining data from different metal ions bound to otherwise identical tags and
543 tagging sites. In the present work, simplifying the NMR spectrum of tryptophan residues by
544 site-selective isotope labelling proved to be of great value for sufficiently improving the
545 spectral resolution to allow assigning the labelled resonances solely from PCSs and PREs. The
546 strategy opens a path to detailed structural investigations of proteins of limited stability like
547 IMP-1, for which complete assignments of the NMR spectrum are difficult to obtain.

548

549

550 **Code and data availability.** NMR spectra and pulse programs are available at
551 <https://doi.org/10.5281/zenodo.5518294>. The script for calculating localisation spaces is
552 available at <https://doi.org/10.5281/zenodo.3594568> and from the GitHub site of Paramagpy.

553

554 **Supplement.** The supplement related to this article is available online at: <https://doi.org/...>

555

556 **Author contributions.** GO initiated the project and edited the final version of the manuscript.
557 HWO wrote NMR pulse programs and software to calculate localisation spaces and performed
558 the $\Delta\chi$ tensor and structure analysis. IDH made labelled protein samples, recorded and assigned
559 NMR spectra, measured PCSs and wrote the first version of the manuscript. AM synthesised
560 the isotope-labelled indole. SJ made ^{15}N -labelled protein mutants with C2 tags and assigned
561 PCSs of backbone amides. MS synthesized C2 tags with different lanthanoid ions. CB, LT and
562 SB synthesized C12 tags with different lanthanoid ions.

563

564 **Competing interests.** The authors declare that they have no conflict of interest.

565

566 **Financial support.** GO thanks the Australian Research Council for a Laureate Fellowship
567 (grant no. FL170100019) and project funding through the Centre of Excellence for Innovations
568 in Peptide and Protein Science, Australian Research Council (grant no. CE200100012). AM
569 thanks the European Regional Development Fund (ERDF) for funding (PostDoc project
570 No. [1.1.1.2/VIAA/2/18/381](https://doi.org/10.1016/j.vaa.2018.03.001)).

571 **References**

572 Arakawa, Y., Murakami, M., Suzuki, K., Ito, H., Wacharotayankun, R., Ohsuka, S., Kato, N.,
573 and Ohta, M.: A novel integron-like element carrying the metallo- β -lactamase gene *bla*_{IMP},
574 *Antimicrob. Agents Chemother.*, 39, 1612–1615, <https://doi.org/10.1128/AAC.39.7.1612>,
575 1995.

576 Bertini, I., Janik, M. B. L., Lee, Y. M., Luchinat, C., and Rosato, A.: Magnetic susceptibility
577 tensor anisotropies for a lanthanide ion series in a fixed protein matrix, *J. Am. Chem. Soc.*,
578 123, 4181–4188, <https://doi.org/10.1021/ja0028626>, 2001.

579 Brem, J., van Berkel, S. S., Zollman, D., Lee, S. Y., Gileadi, O., McHugh, P. J., Walsh, T. R.,
580 McDonough, M.A., and Schofield, C. J.: Structural basis of metallo- β -lactamase inhibition
581 by captopril stereoisomers, *Antimicrob. Agents Chemother.*, 60, 142–150,
582 <https://doi.org/10.1128/AAC.01335-15>, 2016.

583 Brewer, K. D., Bacaj, T., Cavalli, A., Camilloni, C., Swarbrick, J. D., Liu, J., Zhou, A., Zhou,
584 P., Barlow, N., Xu, J., Seven, A. B., Prinslow, E. A., Voleti, R., Häussinger, D., Bonvin, A.
585 M. J. J., Tomchick, D. R., Vendruscolo, M., Graham, B., Südhof, T. C., and Rizo, J.:

586 Dynamic binding mode of a synaptotagmin-1-SNARE complex in solution, Nat. Struct.
587 Mol. Biol., 22, 555–564, <https://doi.org/10.1038/nsmb.3035>, 2015.

588 Bush, K.: Proliferation and significance of clinically relevant β -lactamases, Ann. N. Y. Acad.
589 Sci., 1277, 84–90, <https://doi.org/10.1111/nyas.12023>, 2013.

590 Bush, K.: Alarming β -lactamase-mediated resistance in multidrug-resistant
591 *Enterobacteriaceae*, Curr. Opin. Microbiol., 13, 558–564,
592 <https://doi.org/10.1016/j.mib.2010.09.006>, 2010.

593 Carruthers, T. J.: Paramagnetism & Structural Biology: Biochemical & Biophysical Analysis
594 of IMP-1 Metallo- β -lactamase, PhD thesis, The Australian National University, Canberra,
595 221 pp., 2014.

596 Carruthers, T. J., Carr, P. D., Loh, C.-T., Jackson, C. J., and Otting, G.: Fe³⁺ located in the
597 dinuclear metallo- β -lactamase IMP-1 by pseudocontact shifts. Angew. Chemie Int. Ed., 53,
598 14269–14272, <https://doi.org/10.1002/anie.201408693>, 2014.

599 Chen, W.-N., Nitsche, C., Pilla, K. B., Graham, B., Huber, T., Klein, C. D., and Otting, G.:
600 Sensitive NMR approach for determining the binding mode of tightly binding ligand
601 molecules to protein targets, J. Am. Chem. Soc., 138, 4539–4546,
602 <https://doi.org/10.1021/jacs.6b00416>, 2016.

603 Concha, N. O., Rasmussen, B. A., Bush, K., and Herzberg, O.: Crystal structure of the wide-
604 spectrum binuclear zinc β -lactamase from *Bacteroides fragilis*, Structure, 4, 823–836,
605 [https://doi.org/10.1016/S0969-2126\(96\)00089-5](https://doi.org/10.1016/S0969-2126(96)00089-5), 1996.

606 Concha, N. O., Janson, C. A., Rowling, P., Pearson, S., Cheever, C. A., Clarke, B. P., Lewis,
607 C., Galleni, M., Frere, J.-M., Payne, D. J., Bateson, J. H., and Abdel-Meguid, S. S.: Crystal
608 Structure of the IMP-1 metallo- β -lactamase from *Pseudomonas aeruginosa* and its complex
609 with a mercaptocarboxylate inhibitor: binding determinants of a potent, broad-spectrum
610 inhibitor, Biochemistry, 39, 4288–4298, <https://doi.org/10.1021/bi992569m>, 2000.

611 Crick, D. J., Wang, J. X., Graham, B., Swarbrick, J. D., Mott, H. R., and Nietlispach, D.:
612 Integral membrane protein structure determination using pseudocontact shifts, J. Biomol.
613 NMR, 61, 197–207, <https://doi.org/10.1007/s10858-015-9899-6>, 2015.

614 de la Cruz, L., Nguyen, T.H.D., Ozawa, K., Shin, J., Graham, B., Huber, T., and Otting, G.:
615 Binding of low-molecular weight inhibitors promotes large conformational changes in the
616 dengue virus NS2B-NS3 protease: fold analysis by pseudocontact shifts, J. Am. Chem. Soc.,
617 133, 19205–19215, <https://doi.org/10.1021/ja208435s>, 2011.

618 Galleni, M., Lamotte-Brasseur, J., Rossolini, G. M., Spencer, J., Dideberg, O., Frère, J.-M.,
619 and The Metallo- β -Lactamase Working Group: Standard numbering scheme for class B β -
620 lactamases. *Antimicrob. Agents Chemother.*, 45, 660–663,
621 <https://doi.org/10.1128/AAC.45.3.660-663.2001>, 2001.

622 Gianquinto, E., Tondi, D., D'Arrigo, G., Lazzarato, L., and Spyrakis, F.: Can we exploit β -
623 lactamases intrinsic dynamics for designing more effective inhibitors? *Antibiotics*, 9, 833,
624 <https://doi.org/10.3390/antibiotics9110833>, 2020.

625 González, M. M., Abriata, L. A., Tomatis, P. E., and Vila, A. J.: Optimization of
626 conformational dynamics in an epistatic evolutionary trajectory, *Mol. Biol. Evol.*, 33, 1768–
627 1776, <https://doi.org/10.1093/molbev/msw052>, 2016.

628 Graham, B., Loh, C.T., Swarbrick, J.D., Ung, P., Shin, J., Yagi, H., Jia, X., Chhabra, S.,
629 Pintacuda, G., Huber, T., and Otting, G.: A DOTA-amide lanthanide tag for reliable
630 generation of pseudocontact shifts in protein NMR spectra, *Bioconjugate Chem.*, 22, 2118–
631 2125, <https://doi.org/10.1021/bc200353c>, 2011.

632 Guan, J. Y., Keizers, P. H. J., Liu, W. M., Löhr, F., Skinner, S. P., Heeneman, E. A., Schwalbe,
633 H., Ubbink, M., and Siegal, G.: Small-molecule binding sites on proteins established by
634 paramagnetic NMR spectroscopy. *J. Am. Chem. Soc.*, 135, 5859–5868,
635 <https://doi.org/10.1021/ja401323m>, 2013.

636 Herath, I. D., Breen, C., Hewitt, S. H., Berki, T. R., Kassir, A. F., Dodson, C., Judd, M., Jabar,
637 S., Cox, N., Otting, G., and Butler, S. J.: A chiral lanthanide tag for stable and rigid
638 attachment to single cysteine residues in proteins for NMR, EPR and time-resolved
639 luminescence studies, *Chem. Eur. J.*, 27, 13009–13023,
640 <https://doi.org/10.1002/chem.202101143>, 2021.

641 Hinchliffe, P., González, M. M., Mojica, M. F., González, J. M., Castillo, V., Saiz, C.,
642 Kosmopoulou, M., Tooke, C. L., Llarrull, L. I., Mahler, G., and Bonomo, R. A.: Cross-class
643 metallo- β -lactamase inhibition by bithiazolidines reveals multiple binding modes, *Proc.*
644 *Nat. Acad. Sci.*, 113, E3745–E3754, <https://doi.org/10.1073/pnas.1601368113>, 2016.

645 Hinchliffe, P., Tanner, C. A., Krismanich, A. P., Labbé, G., Goodfellow, V. J., Marrone, L.,
646 Desoky, A. Y., Calvopiña, K., Whittle, E. E., Zeng, F., and Avison, M. B.: Structural and
647 kinetic studies of the potent inhibition of metallo- β -lactamases by 6-
648 phosphonomethylpyridine-2-carboxylates, *Biochemistry*, 57, 1880–1892,
649 <https://doi.org/10.1021/acs.biochem.7b01299>, 2018.

650 Hiraiwa, Y., Saito, J., Watanabe, T., Yamada, M., Morinaka, A., Fukushima, T., and Kudo, T.:
651 X-ray crystallographic analysis of IMP-1 metallo- β -lactamase complexed with a 3-
652 aminophthalic acid derivative, structure-based drug design, and synthesis of 3,6-
653 disubstituted phthalic acid derivative inhibitors, *Bioorg. Med. Chem. Lett.*, 24, 4891–4894,
654 <https://doi.org/10.1016/j.bmcl.2014.08.039>, 2014.

655 Huntley, J.J.A., Scrofani, S.D.B., Osborne, M.J., Wright, P.E., and Dyson, H.J.: Dynamics of
656 the metallo- β -lactamase from *Bacteroides fragilis* in the presence and absence of a tight-
657 binding inhibitor, *Biochemistry*, 39, 13356–13364, <https://doi.org/10.1021/bi001210r>,
658 2000.

659 Huntley, J. J. A., Fast, W., Benkovic, S. J., Wright, P. E., and Dyson, H. J.: Role of a solvent-
660 exposed tryptophan in the recognition and binding of antibiotic substrates for a metallo- β -
661 lactamase, *Protein Sci.*, 12, 1368–1375, <https://doi.org/10.1110/ps.0305303>, 2003.

662 Ito, H., Arakawa, Y., Ohsuka, S., Wachorotayankun, R., Kato, N., and Ohta, M.: Plasmid-
663 mediated dissemination of the metallo- β -lactamase gene *bla*_{IMP} among clinically isolated
664 strains of *Serratia marcescens*, *Antimicrob. Agents Chemother.*, 39, 824–829,
665 <https://doi.org/10.1128/AAC.39.4.824>, 1995.

666 John, M., Park, A. Y., Pintacuda, G., Dixon, N. E., and Otting, G.: Weak alignment of
667 paramagnetic proteins warrants correction for residual CSA effects in measurements of
668 pseudocontact shifts, *J. Am. Chem. Soc.*, 127, 17190–17191,
669 <https://doi.org/10.1021/ja0564259>, 2005.

670 John, M., Park, A. Y., Pintacuda, G., Dixon, N. E., and Otting, G.: Weak alignment of
671 paramagnetic proteins warrants correction for residual CSA effects in measurements of
672 pseudocontact shifts, *J. Am. Chem. Soc.*, 127, 17190–17191,
673 <https://doi.org/10.1021/ja0564259>, 2005.

674 Joss, D., Walliser, R. M., Zimmermann, K., and Häussinger, D.: Conformationally locked
675 lanthanide chelating tags for convenient pseudocontact shift protein nuclear magnetic
676 resonance spectroscopy, *J. Biomol. NMR*, 72, 29–38, [https://doi.org/10.1007/s10858-018-
677 0203-4](https://doi.org/10.1007/s10858-018-0203-4), 2018.

678 Keizers, P. H. J., Saragliadis, A., Hiruma, Y., Overhand, M., and Ubbink, M.: Design,
679 synthesis, and evaluation of a lanthanide chelating protein probe: CLaNP-5 yields
680 predictable paramagnetic effects independent of environment, *J. Am. Chem. Soc.*, 130,
681 14802–14812, <https://doi.org/10.1021/ja8054832>, 2008.

682 Keizers, P. H. J., Mersinli, B., Reinle, W., Donauer, J., Hiruma, Y., Hannemann, F., Overhand,
683 M., Bernhardt, R., and Ubbink, M.: A solution model of the complex formed by adrenodoxin
684 and adrenodoxin reductase determined by paramagnetic NMR spectroscopy, *Biochemistry*,
685 49, 6846–6855, <https://doi.org/10.1021/bi100598f>, 2010.

686 Kobashigawa, Y., Saio, T., Ushio, M., Sekiguchi, M., Yokochi, M., Ogura, K., and Inagaki, F.:
687 Convenient method for resolving degeneracies due to symmetry of the magnetic
688 susceptibility tensor and its application to pseudo contact shift-based protein-protein
689 complex structure determination, *J. Biomol. NMR*, 53, 53–63,
690 <https://doi.org/10.1007/s10858-012-9623-8>, 2012.

691 Laraki, N., Galleni, M., Thamm, I., Riccio, M. L., Amicosante, G., Frère, J.-M., and Rossolini,
692 G. M.: Structure of In101, a *bla*_{IMP}-containing *Pseudomonas aeruginosa* integron
693 phylogenically related to In5, which carries an unusual array of gene cassettes, *Antimicrob.*
694 *Agents Chemother.*, 43, 890–901, <https://doi.org/10.1128/AAC.43.4.890>, 1999a.

695 Laraki, N., Franceschini, N., Rossolini, G. M., Santucci, P., Meunier, C., De Pauw, E.,
696 Amicosante, G., Frère, J.-M., and Galleni, M.: Biochemical characterization of the
697 *Pseudomonas aeruginosa* 101/1477 metallo- β -lactamase IMP-1 produced by *Escherichia*
698 *coli*, *Antimicrob. Agents Chemother.*, 43, 902–906, <https://doi.org/10.1128/AAC.43.4.902>,
699 1999b.

700 Lescanne, M., Ahuja, P., Blok, A., Timmer, M., Akerud, T., and Ubbink, M.: Methyl group
701 reorientation under ligand binding probed by pseudocontact shifts, *J. Biomol. NMR*, 71,
702 275–285, <https://doi.org/10.1007/s10858-018-0190-5>, 2018.

703 Linciano, P., Cendron, L., Gianquinto, E., Spyarakis, F., and Tondi, D.: Ten years with New
704 Delhi metallo- β -lactamase-1 (NDM-1): from structural insights to inhibitor design, *ACS*
705 *Infect. Dis.* 5, 9–34, <https://doi.org/10.1021/acsinfecdis.8b00247>, 2018.

706 Maleckis, A., Herath, I. D., and Otting, G.: Synthesis of ¹³C/¹⁹F/²H labeled indoles for use as
707 tryptophan precursors for protein NMR spectroscopy, *Org. Biomol. Chem.*, 19, 5133–5147,
708 <https://doi.org/10.1039/D1OB00611H>, 2021.

709 Man, B., Su, X.-C., Liang, H., Simonsen, S., Huber, T., Messerle, B. A., and Otting, G.: 3-
710 Mercapto-2,6-pyridinedicarboxylic acid, a small lanthanide-binding tag for protein studies
711 by NMR spectroscopy, *Chem. Eur. J.*, 16, 3827–3832,
712 <https://doi.org/10.1002/chem.200902904>, 2010.

713 Markley, J. L., Bax, A., Arata, Y., Hilbers, C. W., Kaptein, R., Sykes, B. D., Wright, P. E., and
714 Wüthrich, K.: Recommendations for the presentation of NMR structures of proteins and

715 nucleic acids - IUPAC-IUBMB-IUPAB Inter-Union Task Group on the Standardization of
716 Data Bases of Protein and Nucleic Acid Structures Determined by NMR Spectroscopy, J.
717 Biomol. NMR, 12, 1–23, <https://doi.org/10.1023/A:1008290618449>, 1998.

718 Meissner, A., Duus, J. Ø., and Sørensen, O. W.: Spin-state-selective excitation. Application for
719 E.COSY-type measurement of J_{HH} coupling constants, J. Magn. Reson., 128, 92–97,
720 <https://doi.org/10.1006/jmre.1997.1213>, 1997.

721 Moali, C., Anne, C., Lamotte-Brasseur, J., Gros Lambert, S., Devreese, B., Van Beeumen, J.,
722 Galleni, M., and Frère, J.M.: Analysis of the importance of the metallo- β -lactamase active
723 site loop in substrate binding and catalysis, Chemistry & Biology, 10, 319–329,
724 [https://doi.org/10.1016/S1074-5521\(03\)00070-X](https://doi.org/10.1016/S1074-5521(03)00070-X), 2003.

725 Orton, H. W., Huber, T., and Otting, G.: Paramagpy: software for fitting magnetic
726 susceptibility tensors using paramagnetic effects measured in NMR spectra, Magn.
727 Reson., 1, 1–12, <https://doi.org/10.5194/mr-1-1-2020>, 2020.

728 Palacios, A. R., Mojica, M. F., Giannini, E., Taracila, M. A., Bethel, C. R., Alzari, P. M., Otero,
729 L. H., Klinke, S., Llarrull, L. I., Bonomo, R. A., and Vila, A. J.: The reaction mechanism of
730 metallo- β -lactamases is tuned by the conformation of an active-site mobile loop,
731 Antimicrob. Agents Chemother, 63, e01754-18, <https://doi.org/10.1128/AAC.01754-18>,
732 2019.

733 Payne, D. J., Hueso-Rodriguez, J. A., Boyd, H., Concha, N. O., Janson, C. A., Gilpin, M.,
734 Bateson, J. H., Cheever, C., Niconovich, N. L., Pearson, S., Rittenhouse, S., Tew, D., Díez,
735 E., Pérez, P., de la Fuente, J., Rees, M., and Rivera-Sagredo, A.: Identification of a series of
736 tricyclic natural products as potent broad-spectrum inhibitors of metallo- β -lactamases,
737 Antimicrob. Agents Chemother., 46, 1880–1886, [https://doi.org/10.1128/AAC.46.6.1880-](https://doi.org/10.1128/AAC.46.6.1880-1886.2002)
738 [1886.2002](https://doi.org/10.1128/AAC.46.6.1880-1886.2002), 2002.

739 Pearce, B. J. G., Jabar, S., Loh, C. T., Szabo, M., Graham, B., and Otting, G.: Structure
740 restraints from heteronuclear pseudocontact shifts generated by lanthanide tags at two
741 different sites, J. Biomol. NMR, 68, 19–32, <https://doi.org/10.1007/s10858-017-0111-z>,
742 2017.

743 Pilla, K. B., Otting, G., and Huber, T.: Protein structure determination by assembling super-
744 secondary structure motifs using pseudocontact shifts, Structure, 25, 559–568,
745 <https://doi.org/10.1016/j.str.2017.01.011>, 2017.

746 Pintacuda, G., Park, A. Y., Keniry, M. A., Dixon, N. E., and Otting, G.: Lanthanide labeling
747 offers fast NMR approach to 3D structure determinations of protein-protein complexes, *J.*
748 *Am. Chem. Soc.*, 128, 3696–3702, <https://doi.org/10.1021/ja057008z>, 2006.

749 Rossi, M.-A., Martinez, V., Hinchliffe, P., Mojica, M. F., Castillo, V., Moreno, D. M., Smith,
750 R., Spellberg, B., Drusano, G. L., Banchio, C., Bonomo, R. A., Spencer, J., Vila, A. J., and
751 Mahler, G.: 2-Mercaptomethyl-thiazolidines use conserved aromatic–S interactions to
752 achieve broad-range inhibition of metallo- β -lactamases, *Chem. Sci.*, 12, 2898–2908,
753 <https://doi.org/10.1039/d0sc05172a>, 2021.

754 Salimraj, R., Hinchliffe, P., Kosmopoulou, M., Tyrrell, J. M., Brem, J., van Berkel, S. S.,
755 Verma, A., Owens, R. J., McDonough, M. A., Walsh, T. R., Schofield, C. J., and Spencer,
756 J.: Crystal structures of VIM-1 complexes explain active site heterogeneity in VIM-class
757 metallo- β -lactamases, *FEBS J.*, 286, 169–183, <https://doi.org/10.1111/febs.14695>, 2018.

758 Shishmarev, D. and Otting, G.: How reliable are pseudocontact shifts induced in proteins and
759 ligands by mobile paramagnetic metal tags? A modelling study, *J. Biomol. NMR*, 56, 203–
760 216, <https://doi.org/10.1007/s10858-013-9738-6>, 2013.

761 Softley, C. A., Zak, K. M., Bostock, M. J., Fino, R., Zhou, R. X., Kolonko, M., Mejdj-Nitiu,
762 R., Meyer, H., Sattler, M., and Popowicz, G. M.: Structure and molecular recognition
763 mechanism of IMP-13 metallo- β -lactamase, *Antimicrob. Agents Chemother.*, 64, e00123-
764 20, <https://doi.org/10.1128/AAC.00123-20>, 2020.

765 Su, X.-C., McAndrew, K., Huber, T., and Otting, G.: Lanthanide-binding peptides for NMR
766 measurements of residual dipolar couplings and paramagnetic effects from multiple angles,
767 *J. Am. Chem. Soc.*, 130, 1681–1687, <https://doi.org/10.1021/ja076564l>, 2008.

768 Toney, J. H., Hammond, G. G., Fitzgerald, P. M., Sharma, N., Balkovec, J. M., Rouen, G. P.,
769 Olson, S. H., Hammond, M. L., Greenlee, M. L., and Gao, Y. D.: Succinic acids as potent
770 inhibitors of plasmid-borne IMP-1 metallo- β -lactamase, *J. Biol. Chem.*, 276, 31913–31918,
771 <https://doi.org/10.1074/jbc.M104742200>, 2001.

772 van Duin, D., Kaye, K. S., Neuner, E. A., and Bonomo, R. A.: Carbapenem-resistant
773 Enterobacteriaceae: a review of treatment and outcomes, *Diagn. Microbiol. Infect. Dis.* 75,
774 115–120, <https://doi.org/10.1016/j.diagmicrobio.2012.11.009>, 2013.

775 Wachino, J., Kanechi, R., Nishino, E., Mochizuki, M., Jin, W., Kimura, K., Kurosaki, H., and
776 Arakawa, Y.: 4-Amino-2-sulfanylbenzoic acid as a potent subclass B3 metallo- β -lactamase-
777 specific inhibitor applicable for distinguishing metallo- β -lactamase subclasses, *Antimicrob.*
778 *Agents Chemother.* 63, e01197-19, <https://doi.org/10.1128/AAC.01197-19>, 2019.

779 Watanabe, M., S. Iyobe, M. Inoue, and S. Mitsuhashi: Transferable imipenem resistance in
780 *Pseudomonas aeruginosa*, *Antimicrob. Agents Chemother.* 35, 147–151, [https://doi.org/](https://doi.org/10.1128/AAC.35.1.147)
781 10.1128/AAC.35.1.147, <https://doi.org/10.1128/AAC.35.1.147>, 1991.

782 Yagi, H., Pilla, K. B., Maleckis, A., Graham, B., Huber, T., and Otting, G.: Three-dimensional
783 protein fold determination from backbone amide pseudocontact shifts generated by
784 lanthanide tags at multiple sites, *Structure*, 21, 883–890,
785 <https://doi.org/10.1016/j.str.2013.04.001>, 2013.

786 Yamaguchi, Y., Matsueda, S., Matsunaga, K., Takashio, N., Toma-Fukai, S., Yamagata, Y.,
787 Shibata, N., Wachino, J., Shibayama, K., Arakawa, Y., and Kurosaki, H.: Crystal structure
788 of IMP-2 metallo- β -lactamase from *Acinetobacter* spp.: comparison of active-site loop
789 structures between IMP-1 and IMP-2, *Biol. Pharm. Bull.* 38, 96–
790 101, <https://doi.org/10.1248/bpb.b14-00594>, 2015.

791 Yamaguchi, Y., Kato, K., Ichimaru, Y., Jin, W., Sakai, M., Abe, M., Wachino, J., Arakawa,
792 Y., Miyagi, Y., Imai, M., Fukuishi, N., Yamagata, Y., Otsuka, M., Fujita, M., and Kurosaki,
793 H.: Crystal structures of metallo- β -lactamase (IMP-1) and its D120E mutant in complexes
794 with citrate and the inhibitory effect of the benzyl group in citrate monobenzyl ester, *J. Med.*
795 *Chem.*, 64, 10019–10026, <https://doi.org/10.1021/acs.jmedchem.1c00308>, 2021.

796 Yamaguchi, H., M. Nukaya, and T. Sawai, T: Sequence of *Klebsiella pneumoniae* RDK4
797 metallo- β -lactamase, EMBO database accession no. D29636, EMBO, Heidelberg,
798 Germany, 1994.

799 Zimmermann, K., Joss, D., Müntener, T., Nogueira, E. S., Schäfer, M., Knörr, L., Monnard,
800 F. W., and Häussinger, D.: Localization of ligands within human carbonic anhydrase II
801 using ^{19}F pseudocontact shift analysis, *Chem. Sci.*, 10, 5064–5072,
802 <https://doi.org/10.1039/c8sc05683h>, 2019.